CHEMISTRY
A European Journal

A Journal of
ChemPubSoc Europe

Accepted Article

Title: Solvent Dependent Nanostructures Based on Active π-Aggregation Induced Emission Enhancement of New Carbazole Derivatives of Triphenylacrylonitrile

Authors: Santu Maity, Krishnendu Aich, Chandraday Prodhan, Keya Chaudhuri, Ajoy Kumar Pramanik, Siddhartha Das, and Jhuma Ganguly

To be cited as: *Chem. Eur. J.* 10.1002/chem.201900312

Link to VoR: http://dx.doi.org/10.1002/chem.201900312

Supported by
ACES

WILEY-VCH

Solvent Dependent Nanostructures Based on Active π-Aggregation Induced Emission Enhancement of New Carbazole Derivatives of Triphenylacrylonitrile

Santu Maity,[a] Krishnendu Aich,[a] Chandraday Prodhan,[b] Keya Chaudhuri,[b] Ajoy Kumar Pramanik,[c] Siddhartha Das,[d] and Jhuma Ganguly*[a]

Abstract: In the present study, the carbazole and 2,3,3-triphenylacrylonitrile (TPAN) nanostructures (2-CTPAN and 2,2'-CTPAN) have been designed and synthesized by Pd-catalyzed Sonogashira cross-coupling reaction. CTPAN exhibit aggregation induced emission enhancement (AIEE) behaviour in water with high fluorescence quantum yield. Both the compounds show tunable self-assembly in water as well as in dimethylformamide (DMF) by extended π-π stacking interaction. CTPAN can be self-assembled into spherical particles in water and the structures of these self-assemblies have been investigated using X-ray diffraction. Interestingly, 2-CTPAN and 2,2'-CTPAN form organogels with a critical gelation concentration (CGC) of 11 and 15 mg/mL, respectively, in DMF and exhibit acicular and rod shaped morphology, respectively. The single crystal structure of 2-CTPAN shows that the intermolecular C-H···π interactions lock the molecular conformation into a staircase-shaped supramolecular assembly. These AIEE active compounds reveal high water dispersibility, strong yellow fluorescence with high quantum yield, promising photostability and excellent biocompatibility which make them a potential bio-imaging agent.

Introduction

The development of novel fluorescent nanoparticle based bio-imaging probes have created new avenues in interdisciplinary fields that range from biology to materials science.[1] Their remarkable optical properties make them promising for drug delivery, bioanalysis, bio-imaging and other biomedical applications.[2-4] Previously, a large number of inorganic fluorescent nanoparticles including quantum dots, silicon quantum dots, carbon dots, fluorescent metal clusters and Ln^{3+}-ion doped nanomaterials have been extensively explored for bio/chemosensors applications.[5-11] In spite of the advantages of strong fluorescence intensity and limited dosage, fluorescent inorganic nanoparticles have many inherent disadvantages for biomedical applications, such as relatively laborious synthesis, difficult to tune fluorescence, potential toxicity due to their accumulation in the reticuloendothelial system (RES) after intravenous injection, blinking effect, poor biodegradability and non-functionalized hydrophobic entities.[12,13] Fluorescent proteins are also a class of bioprobes which also have limited applications due to their high cost, low molar absorptivity and low photobleaching thresholds.[14] On the other hand, organic dyes and conventional fluorescent organic nanoparticles (FONs) exhibit aggregation caused quenching (ACQ) issue, poor membrane permeability and easy photo-bleaching.[15-17] Besides, the photostability is very important for protracted observation, where photobleaching rigorously affects the capability to sense the target molecules.[18,19]

Thus, novel fluorescent nanoparticles FNPs with good biocompatibility and low cytotoxicity are still in urgent pursuit.[20,21] Recent advancements on the unique aggregation induced emission (AIE) based materials open up a new opportunity for the preparation of the organic molecule based fluorescent nanoprobes.[22-26] Till date, a large number of AIE active molecules with different chemical characteristics have been discovered and utilized for fabrication of AIE-active FONs including naphthalene–diimide, tetraphenylethene (TPE), siloles, PEGylated carbazole and some metal complexes.[27-32] Such probes have been used as fluorescent tools for the detection of biomolecules and biochemical events, imaging agent in live cells, organic light-emitting devices and chemosensors.[33-35]

AIE active molecules can be transformed into functionalized nanoparticles with their varied applications in biomedical field.[36] With the intention to develop AIE based nanoparticles, several approaches have been reported yet. The simplest approach is the incorporation of AIE moiety into the self-assembled/aggregated structure of the polymers or molecules and it has emerged as a fascinating aspect owing to their optimum flexibility, extensive π–π interaction, and the feasibility of peripheral modification with various functional groups for enhanced intermolecular interactions.[37-39] Size of these nanoparticles have been controlled between 25 to 300 nm for successful biomedical applications.[2]

Though, there has been a significant progress in the AIE active nanoprobes, there are still several issues for their wider applications. Firstly, the presence of non-AIE molecule/polymer in the core of AIE-based nanoparticle makes its fluorescence property highly dependent on the amount of AIE molecule. Secondly, synthesis of fluorescent nanoparticle of controlled size is very difficult by these methods due to the existence of non-AIE materials. Thirdly, most of these nanoparticles have low colloidal stability and frequently lose their assembled structure. Fourthly, a very few number of functionalization has been

[a] Mr. S. Maity, Dr. K. Aich, Dr. J. Ganguly
Department of Chemistry, Indian Institute of Engineering Science and Technology, Howrah-711103, India
E-mail: jhumaiiest@gmail.com
[b] Mr. C. Prodhan, Prof. Keya Chaudhuri
Molecular Genetics Department, CSIR-Indian Institute of Chemical Biology, Kolkata, 700032, India
[c] Dr. A. K. Pramanik
Department of Chemistry, New Alipore College, University of Calcutta, Kolkata, 700053, India
[d] Prof. S. Das
Department of Metallurgical and Materials Engineering, Indian Institute of Technology, Kharagpur, 721302, India
Supporting information for this article is given via a link at the end of the document.

accomplished with respect to various functional nanoparticle made of inorganic nanoparticles.[2] A comparison table with the reported nanoparticles made by AIE luminogen has been added in the revised supplementary information (Table S1) to show the novelty of the probes.

There are only a few reported literatures about TPAN and carbazole based AIE active probe. Among them, Dong *et al*. investigated AIE and intramolecular charge transfer (ICT) properties of polycarbazoles and polytriphenylamines probes and used them for the detection of 1,3,5-trinitrobenzene (TNB).[40] Zhan *et al*. studied AIE, ICT and mechanofluorochromic properties of carbazole-based triphenylacrylonitrile derivatives.[41] Herein, we present the design and synthesis of substituted carbazole-TPAN based dyes (2-CTPAN and 2,2'-CTPAN) and their AIEE characteristics. The photophysical and self-assembly behaviors of the dyes have been investigated thoroughly. Both the probes show distinct solvent dependent nanostructures in water and DMF. It has been found that both 2-CTPAN and 2,2'-CTPAN form spherical particles of size <200 nm in aqueous medium (THF/Water=1:9), which are strong emissive with a high fluorescence quantum yield (ϕ_f = 7.55% and 13.52% for 2-CTPAN and 2,2'-CTPAN respectively), and has been successfully applied for live cell imaging. 2-CTPAN and 2,2'-CTPAN form organogels in DMF with acicular and rod shaped morphology, respectively. The 2-CTPAN and 2,2'-CTPAN nanoparticles are composed of only AIE molecules and the surface modification of carbazole moiety by TPAN unit can be attained by this approach. Moreover, FONs of 2-CTPAN and 2,2'-CTPAN have good colloidal stability with high fluorescence quantum yield owing to locking of their conformation through intermolecular C-H$\cdots\pi$ and π-π stacking interaction.

Results and Discussion

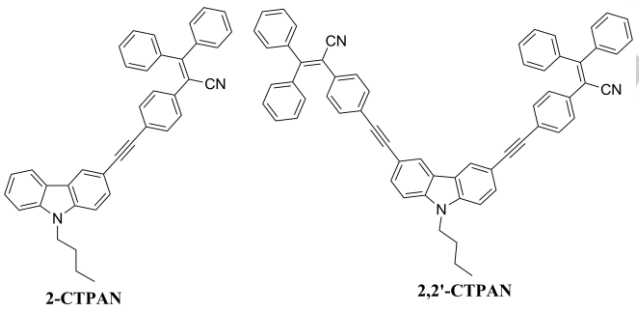

Scheme 1. Structure of 2-CTPAN and 2,2'-CTPAN.

2,3,3-triphenylacrylonitrile (TPAN) was selected as AIE molecule because this molecule was well studied and various chemical functionalization could be easily achieved.[40,41] Chemical structure of the probes (Scheme 1) and the details synthesis approach are shown in Scheme S1. Chemical structures and purities of 2-CTPAN and 2,2'-CTPAN were fully characterized and confirmed by ^{1}H NMR, ^{13}C NMR and HRMS (Figure S1−S6).

The energy dispersive X-ray (EDX) spectroscopy (Figure S7) also confirms the presence of C and N in 2-CTPAN and 2,2'-CTPAN probe.

Photo-physical properties

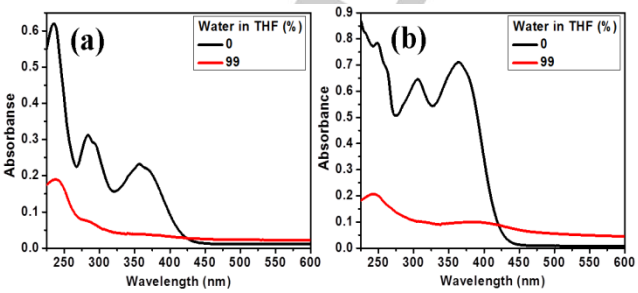

Figure 1. UV-Vis absorption spectrum of (a) 2-CTPAN and (b) 2,2'-CTPAN (concentration: 10μM).

The absorption spectra of 2-CTPAN and 2,2'-CTPAN show diminished absorption with the increase in water content from 0% to 99% in THF solution. Figure 1 confirms that in aggregate state, i.e., in the presence of 99% water tail in absorption spectra is formed. The leveling-off of the tail absorption is attributed to the Mie scattering in aggregate state. In a "good" solvent like THF, sharp absorption bands (λ_{max}) are noticed (Figure 1) at 355 and 362 nm for 2-CTPAN and 2,2'-CTPAN respectively, due to π–π* transitions.[42] From UV-Vis spectra (Figure S8) it can be seen that at 80% and 70% of water fraction aggregation occurs for 2-CTPAN and 2,2'-CTPAN respectively and is responsible for the red shift of the absorption maxima.[43] Above 90% water content, all vibronic features of the spectra got completely lost and the π–π* absorption bands exhibit a significant bathochromic shift. This type of phenomenon is well known for the formation of J-aggregates.[43] AIE properties of 2-CTPAN and 2,2'-CTPAN are shown in Figure 2 and it is clear that their fluorescent properties are dependent on the aggregated microenvironment.[44] The 2-CTPAN and 2,2'-CTPAN are almost non-fluorescent or weakly fluorescents in THF due to their higher solubility in that solvent. However, upon addition of 99% water to THF solution enhanced the emission intensity up to 44-fold (Figure 2), showing a significant AIEE effect and a strong yellow fluorescence appears due to lowering of the solubility of the FONs in the solution. The quantum yield (ϕ_f) of 2-CTPAN and 2,2'-CTPAN are calculated using quinine sulphate as standard (in 0.1M H_2SO_4, ϕ_f = 54%).[41,45] The ϕ_f of 2-CTPAN in 0% and 99% H_2O/THF are 0.52% and 7.55%, respectively, whereas the ϕ_f of 2,2'-CTPAN in 0% and 99% H_2O/THF are 0.36 and 13.52 %, respectively. These results clearly demonstrate that 2-CTPAN and 2,2'-CTPAN exhibit AIEE properties.

The fluorescence decay profiles of 2-CTPAN and 2,2'-CTPAN (Figure 3) have been examined with an excitation using a 370 nm diode and it is fitted to a single exponential. The mean PL lifetime of 2-CTPAN increases from 3 ps in 0% water/THF to 33

ps in 50% water/THF to 2919 ps in 99% water/THF. Similarly, for 2,2'-CTPAN, it increases from 2 ps in 0% water/THF to 32 ps in 50% water/THF to 2542 ps in 99% water/THF. Generally, the lifetime and fluorescence quantum yield of most of the AIEE molecules usually increase after aggregation owing to the activation of the radiative recombination process and/or reduction of non-radiative recombination methods.[46] Consequently, the formation of FONs prevents intramolecular motions, which includes rotation and vibration, in the aggregated state of CTPAN in the excited state.[47] Therefore, the excited molecules immediately release the energy in the form of fluorescence which results in a higher fluorescence quantum yield and longer lifetime.

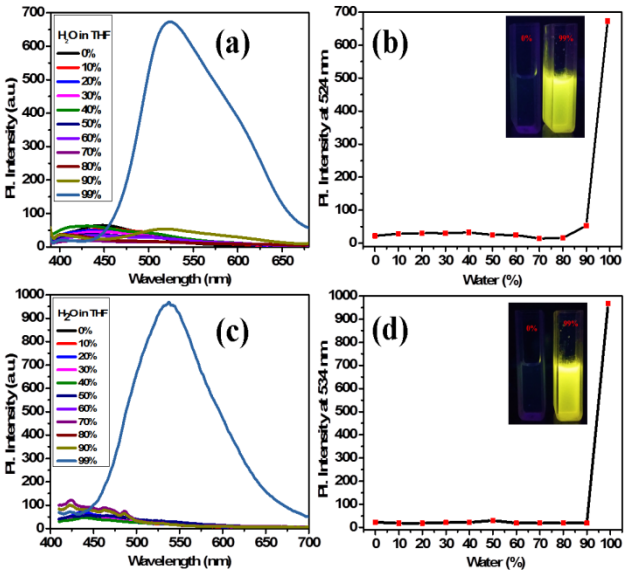

Figure 2. Photoluminescence (Pl) spectra of (a) 2-CTPAN and (c) 2,2'-CTPAN in different fraction of H_2O in THF demonstrating its AIEE property. Plot of the maximum PL intensity vs % of water of (b) 2-CTPAN and (d) 2,2'-CTPAN. Inset: Fluorescent images of (b) 2-CTPAN and (d) 2,2'-CTPAN in 0% and 99% H_2O in THF (conc: 10 μM, λ_{ex}=370 nm for 2-CTPAN and λ_{ex}=390 nm for 2,2'-CTPAN).

The UV-Vis spectra of 2-CTPAN and 2,2'-CTPAN in DMF are given in Figure S9. Both the probes exhibit two characteristic absorption bands. 2-CTPAN and 2,2'-CTPAN show absorptions with shorter/longer-wavelength of ~293/355 and ~305/365 nm, respectively. As the probes are soluble in DMF, controlled aggregation may lead to formation of acicular and rod shaped morphology for 2-CTPAN and 2,2'-CTPAN respectively and the absorption spectra exhibit characteristic π-π* transition. As represented in fluorescence spectra (Figure S10), 2-CTPAN and 2,2'-CTPAN is non-emissive in DMF but both the probe is highly emissive in water.

Moreover, the time dependent DLS study establishes that the prepared FONs (2-CTPAN and 2,2'-CTPAN) present a good colloidal stability (Figure S11) in both PBS and water. Results also suggest that the FONs do not precipitate in PBS buffer and water after they are kept for 60 min and they are still stable in PBS buffer, even after 2 days. The fluorescent images of the prepared nanoparticles are presented in Figure S12 at different time intervals to show the colliodal stability of the FONs.

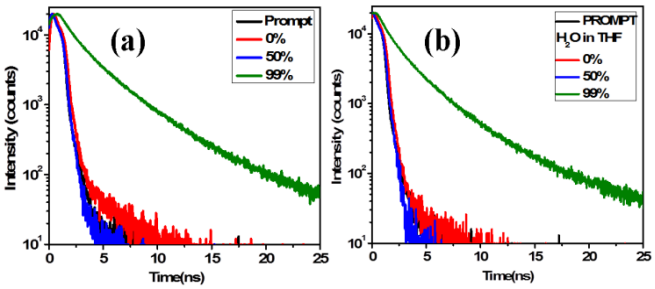

Figure 3. Fluorescence decay profiles of (a) 2-CTPAN and (b) 2,2'-CTPAN using 370 nm diodes (conc: 10 μM, λ_{em}=524 nm for 2-CTPAN and λ_{em}=537 nm for 2,2'-CTPAN).

Microscopic nanostructure

In order to investigate the size and morphology of the 2-CTPAN and 2,2'-CTPAN in the aggregated state, SEM, TEM, fluorescence microscopy and DLS analysis have been carried out. SEM images (Figure 4) reveal the formation of distinguished spherical particles for 2-CTPAN and 2,2'-CTPAN with an average diameter ranging from 100 to 200 nm.[4,48,49] A similar spherical morphology has been also observed in the TEM and fluorescence microscopy images (Figure 4). Therefore, it is evident that the spherical particles are self-assembled in the form of spherical particles. More uniform spherical aggregates were observed in the case of 2,2'-CTPAN owing to the presence of two fold TPAN moiety. From DLS measurements, the average particle size obtained for both sample are 250±10 nm (Figure S11). The difference in average size measured from SEM and DLS is due to the presence of the hydration sphere in the solution phase.

2-CTPAN and 2,2'-CTPAN form light yellow colored gel in DMF with a CGC of 11 and 15 mg/mL at room temperature. TEM (Figure 5) images of the self-assembled organogel of 2-CTPAN and 2,2'-CTPAN reveal an acicular and rod shaped morphology, respectively, which is typical for a gelator. Both in water and DMF, the self-assembly of CTPAN are initially triggered by π-π stacking interaction leading to the formation of an extended aromatic stack with a head-to-head orientation of the unsymmetrical molecules. In water, to avoid unfavorable solvent interaction, they fold to form into spherical particles.

However, in a relatively less polar solvent DMF, the scenario is a bit different as in this case the interaction of the solvent molecule with the carbazole and TPAN may not be as repulsive as that in water. In DMF, 2-CTPAN and 2,2'-CTPAN produces a different self-assembly mode and forms acicular and rod shaped morphology, respectively. The different self-assembly mode of 2-CTPAN in water and DMF is represented in Scheme 2.

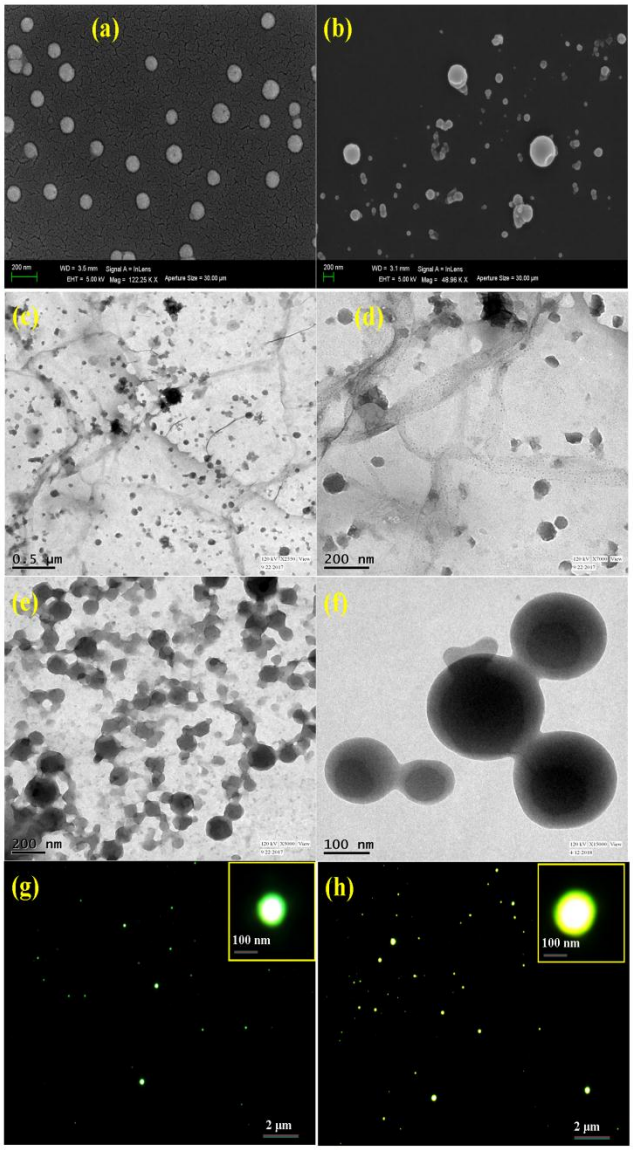

Figure 4. SEM image of (a) 2-CTPAN and (b) 2,2'-CTPAN; TEM images of (c), (d) 2-CTPAN and (e), (f) 2,2'-CTPAN; fluorescence microscopic images of (g) 2-CTPAN and (h) 2,2'-CTPAN (conc: 10 μM).

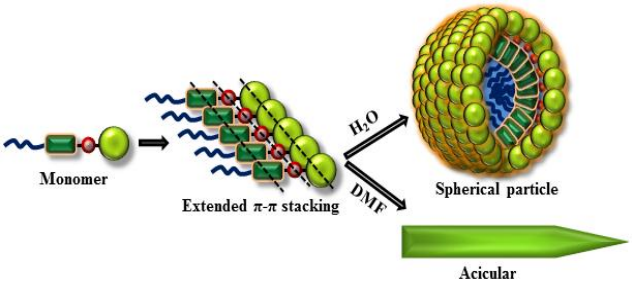

Scheme 2. Proposed scheme of solvent-regulated nanostructures of 2-CTPAN.

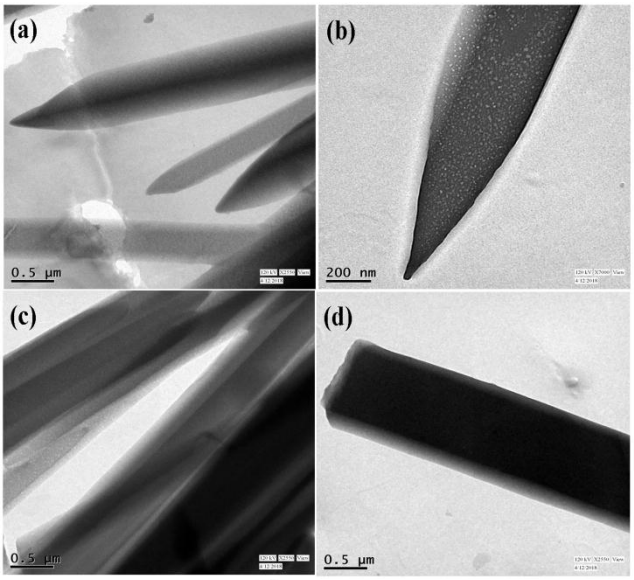

Figure 5. TEM images of organogel of (a), (b) 2-CTPAN and (c), (d) 2,2'-CTPAN, prepared by diluting the gel using DMF.

Molecular arrangement using thin film XRD

To understand the nature of the molecular arrangement in aggregate state, the XRD patterns have been analyzed for both 2-CTPAN and 2,2'-CTPAN (Figure S13). The diffraction patterns of 2-CTPAN consist of five sharp peaks with 2θ values 8.57°, 13.11°, 14.18°, 20.48° and 22.72°, which reflect the d-spacing values of 10.32, 6.75, 6.24, 4.33 and 3.91 Å, respectively. Similarly, 2,2'-CTPAN also comprise of five peaks with 2θ values 9.48°, 13.23°, 13.74°, 20.95° and 27.77°, which corresponds to the d-spacing values of 9.32, 6.69, 6.44, 4.24 and 3.21 Å respectively. Using chem3D Pro 12.0 (Figure S14), the fully extended length of the energy minimized structure of 2-CTPAN and 2,2'-CTPAN has been found to be 22.59 and 25.25 Å respectively. Such a large difference in the theoretical and experimental values suggests that, there must be an intercalation between TPAN units and carbazole units within the π–π stacked CTPAN core. The molecules apparently will arrange in a multilayer head to head fashion, resulting in the formation of J-type aggregates. The sharp reflection peaks observed for 2-CTPAN compared to those of 2,2'-CTPAN indicating an increased crystallinity because of less steric hindrance in the former case. The crystalline nature of 2-CTPAN has also been found in the TEM micrographs (Figure S15).

X-ray crystal structure

Fine and X-ray quality single crystals of yellow colored compound 2-CTPAN was grown by slow diffusion of ethyl acetate solution into methanol (v/v = 1:1) at ambient condition over a week. Crystallographic details for 2-CTPAN is given in

Table S2. The single crystal X-ray diffraction analysis fits well with the expected structure of 2-CTPAN, as shown in Figure 6. The 2, 3, 3-triphenylacrylonitrile unit exhibits the typical Propeller-shaped structure, linked by the alkyne linkage which is co-planar with the carbazole functionalized unit at the extreme rare part of the molecule. The length (Table S3) of the central C22—C23 bond is 1.204(4) Å, which is typical for a C≡C bond. The C15—N1 bond length is 1.134(4) Å, which is comparable with other standard cyanide-containing organic or inorganic compounds.

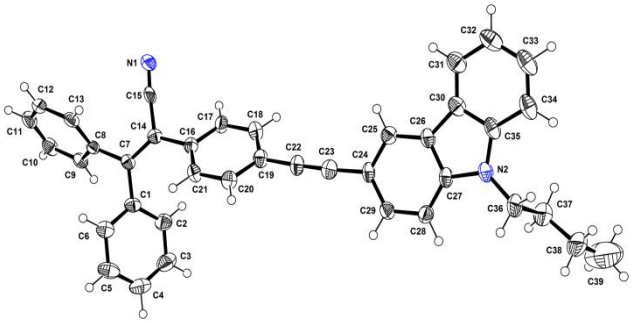

Figure 6. ORTEP structure of 2-CTPAN with 35% thermal ellipsoids probability displacement level for non-H atoms with atom numbering scheme.

Supramolecular features

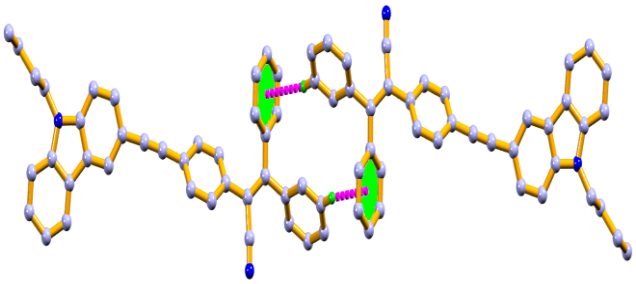

Figure 7. Formation of *edge* to *face* cyclic dimer of 2-CTPAN by aromatic C-H…π(Cg) interaction.

The crystal structure of 2-CTPAN is stabilized by the formation of edge to face cyclic and centrosymmetric dimeric framework through C(10)—H(7)....π Cg(2) (acrylic phenyl centroid) interaction with an overall inversion of symmetry. This intermolecular C-H....π interaction between two molecular units is an eight member dimmer (Figure 7).

Moreover, in addition to the acrylic phenyl dimeric C-H....π interaction, the single crystal structure reveals extensively both aliphatic and aromatic C-H....π interactions (Figure 8) which generate a 1-dimensional supramolecular network along C-axis. The aliphatic C-H....π interaction (Table S4) is built up through alkyne π-electron density of C22—C23 bond and C(18)—H(12) and C(20)—H(13) of the similar acrylic phenyl rings of the dimer forming a staircase-shaped supramolecular association. Aromatic C-H....π interaction is observed between C(2)—H(1)....π Cg(6) (carbazolyl phenyl centroid). These types of inter molecular interactions might rigidify the molecular conformation and prohibit the intramolecular rotation which leads to highly emissive behaviors. From the crystal packing it is also clear that the molecules orient in head-to-tail fashion due to extensive π-π and CH-π interactions which is the typical feactures of J-agreegation.

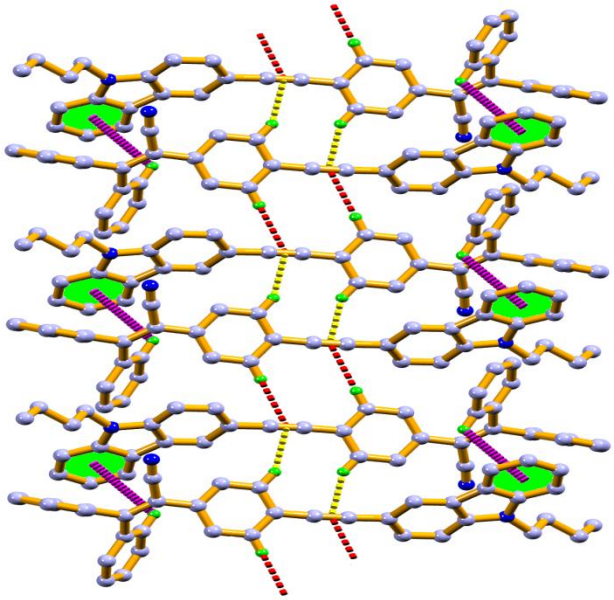

Figure 8. Crystal packing diagram of 2-CTPAN shows a ladder structure involving both aliphatic (in yellow and red color) and aromatic C-H…π (in purple color) interaction viewed along crystallographic c-axis (ab-plane) to from 1-D supramolecular network (H-atoms not involved in interaction are omitted for clarity).

Biological responses

In the present study, the capabilities of the ligands 2-CTPAN and 2,2'-CTPAN have been evaluated to show intracellular fluorescence. The cytotoxic effects of 2-CTPAN and 2,2'-CTPAN have been determined by a cell viability assay in HepG2 cells. Up to 10 μM concentration, there is no significant reduction in the tetrazolium salt reflecting a decrease in formazan production, as the ligand 2-CTPAN shows less than 20% cytotoxicity and more than 85% of cells are viable up to a dose of 5 μM (Figure 9). Therefore, no significant cytotoxicity has been observed up to 10 μM concentration of the 2-CTPAN and further experiments have been carried out with 5 μM and 10 μM of the ligand. Again, for 2,2'-CTPAN, more than 88% cells are viable upto 10 μM concentration for the ligand. Hence, for the intracellular fluorescence study, the cells are treated with 5 μM and 10 μM concentration of the ligand.

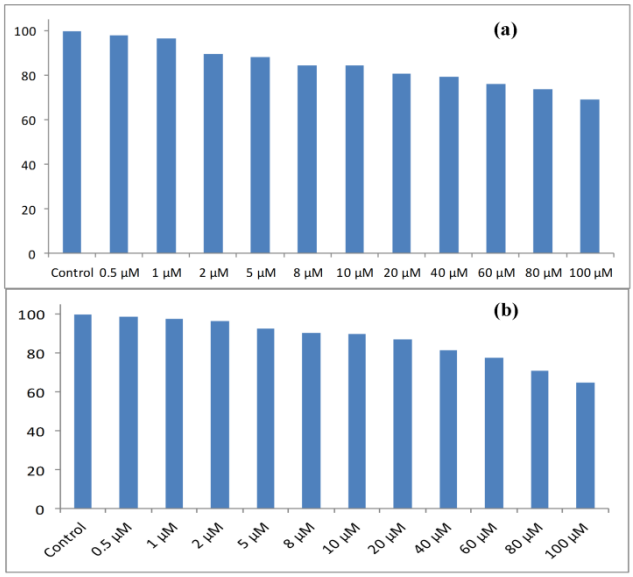

Figure 9. Percent (%) cell viability of HepG2 cells treated with different concentrations (1-100 µM) of (a) 2-CTPAN (b) 2,2'-CTPAN for 24 hours determined by MTT assay.

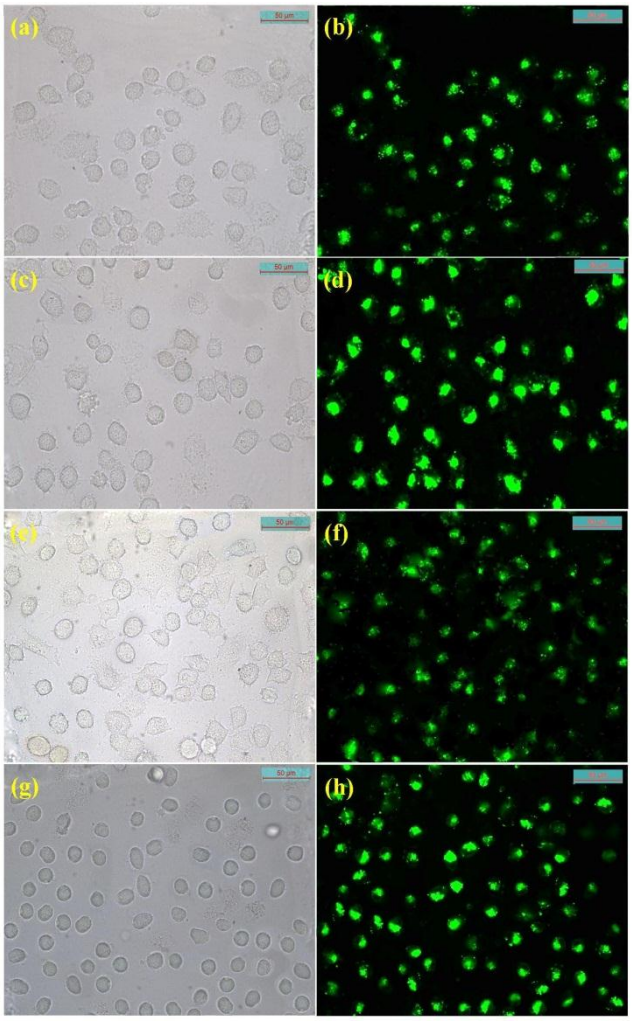

Figure 10. (a), (c) bright field images and (b), (d) fluorescence images treated with 5 and 10 µM 2-CTPAN respectively; (e), (g) bright field images and (f), (h) fluorescence images treated with 5 and 10 µM 2,2'-CTPAN respectively of HepG2 cells. The fluorescence images of HepG2 cells were capture (40X) after incubation with 5µM and 10 µM of 2-CTPAN and 2,2'-CTPAN for 60 min at 37°C, followed by washing thrice with 1X PBS. An excitation filter of 300-500 nm was used. The fluorescence images showed prominent signal by the fluorophore 2-CTPAN and 2,2'-CTPAN at 5 µM concentration, which gradually increased in 10 µM concentration.

Now, taking into consideration the compelling fluorescence property of 2-CTPAN and 2,2'-CTPAN, it has been further checked *in vitro* for intracellular fluorescence signal (Figure 10). Intracellular imaging of HepG2 cells have been treated with 5 µM of the 2-CTPAN and 2,2'-CTPAN which shows prominent blue fluorescence. Increased blue fluorescence emission has been observed inside the cells as the HepG2 cells are incubated with 10 µM of 2-CTPAN and 2,2'-CTPAN for 60 min at 37 °C. The fluorescence images show clear localization of the ligand in the cytoplasmic region. Hence, the present ligand with low cytotoxicity and excellent biocompatibility can be used as potential fluorescent sensors in biological samples.

Conclusions

In summary, new AIEE luminogens based on carbazole modified triphenylacrylonitrile derivatives 2-CTPAN and 2,2'-CTPAN have been designed and synthesized by Pd-catalyzed Sonogashira cross-coupling reaction. The planarization induced extensive π−π stacking and strong D-π-A interaction makes these derivative AIEE active. The presence of the electron withdrawing group (TPAN) into the carbazole moiety induces the red shift in absorption spectra (J-type aggregation) upon increasing solvent polarity from THF to water. The self-assembled nanostructures emit strong yellow fluorescence and show quantum yield as high as 7.55 and 13.52 for 2-CTPAN and 2,2'-CTPAN, respectively, in aggregate state. The AIEE active 2-CTPAN and 2,2'-CTPAN are aggregated into spherical particles of size <200 nm in water. With the change in solvent from water to DMF, their morphology switches to acicular and rod shape geometry for 2-CTPAN and 2,2'-CTPAN, respectively, account for gelation. The single crystal X-ray structure of 2-CTPAN reveals that the intermolecular C-H…π interactions lock the molecular skeleton, which will arrange the molecule into a staircase-shaped supramolecular association. The intracellular imaging of HepG2 cells confirms clear localization of the CTPAN in the cytoplasmic region. These FONs exhibit high water dispersibility, strong fluorescence intensity, excellent biocompatibility and low cytotoxicity which make them promising agent for fluorescent sensors in biological samples. Besides, this work opens a new avenue to use such materials for further biomedical applications including tissue imaging, drug delivery and long term cell tracking.

Experimental Section

Synthesis of compound 1 and 2

Compounds 1 and 2 have been prepared according to reported literature procedure.[50,51]

Preparation of 2-(4-((9-butyl-9H-carbazol-3-yl)ethynyl)phenyl)-3,3-diphenylacrylonitrile (2-CTPAN)

2-(4-bromophenyl)-3,3-diphenylacrylonitrile (500 mg, 1.39 mmol) was dissolved in THF (20 mL) and $Pd(PPh_3)_2Cl_2$ (30 mg, 0.04 mmol), PPh_3 (36 mg, 0.14 mmol) and copper iodide (5 mg) added subsequently to it under argon atmosphere. After 15 min of stirring at room temperature, triethylamine (10 mL) was added to the reaction mixture and the stirring was continued for further 30 min. After that, 9-butyl-3-ethynyl-9H-carbazole (340 mg, 1.39 mmol) was added to it and the reaction mixture was heated at 80 ^{0}C for 6 h. After completion of the reaction all volatile materials were removed under vacuum and the residue was extracted with ethyl acetate (3 × 20 mL). The crude product was purified using column chromatography (silica gel/ethyl acetate : petroleum ether, 1:4) afforded 2-CTPAN (522 mg, Yield = 72%) as a light yellow solid. **^{1}H NMR (500 MHz, $CDCl_3$):** δ 8.27 (s, 1H), 8.11 (d, J = 7.5, 1H), 7.61 (s, 1H), 7.50-7.37 (m, 10H), 7.29-7.22 (m, 6H), 7.06 (t, J = 6.6, 2H), 4.33 (t, J = 7.2, 2H), 1.87 (q, J = 7.2, 2H), 1.43 (q, J = 7.3, 2H), 0.96 (t, J = 7.3, 3H). **^{13}C NMR (100 MHz, $CDCl_3$):** δ 158.15, 140.98, 140.50, 140.39, 139.14, 134.24, 131.54, 130.92, 130.10, 129.80, 129.37, 129.30, 128.61, 128.53, 126.29, 124.25, 124.17, 123.04, 122.56, 120.64, 120.03, 119.54, 112.95, 111.29, 109.10, 108.91, 92.73, 87.30, 43.12, 31.22, 20.66, 13.98. **HRMS (ESI, m/z):** calcd for $C_{39}H_{30}N_2Na$ $(M+Na)^+$, 549.2307; found, 549.2305.

Preparation of 2,2'-(((9-butyl-9H-carbazole-3,6-diyl)bis(ethyne-2,1-diyl))bis(4,1-phenylene))bis(3,3-diphenylacrylonitrile) (2,2'-CTPAN)

2-(4-bromophenyl)-3,3-diphenylacrylonitrile (500 mg, 1.39 mmol), $Pd(PPh_3)_2Cl_2$ (40 mg, 0.057 mmol), PPh_3 (50 mg, 0.19 mmol) and copper iodide (5 mg) were added in THF (15 mL) and stirred for 20 min under argon atmosphere at room temperature. After that, triethylamine (5 mL) was added to it and stirred for another 30 min. Compound 2 (190 mg, 0.7 mmol) was then added to the reaction mixture and heated at 80 ^{0}C for 14 h. Progress of the reaction was monitored by TLC. All volatile materials were removed under vacuum after completion of the reaction and the residue was extracted with dichloromethane (3 × 20 mL). After removal of the solvent, the crude product was purified using column chromatography (ethyl acetate : petroleum ether, 3:7) yielded 2,2'-CTPAN (460 mg, 79%) as yellow solid. **^{1}H NMR (400 Hz, $CDCl_3$):** δ 8.24 (s, 2H), 7.63 (dd, J_1 = 1.2, J_2 = 8.4, 2H), 7.36-7.48 (m, 15H), 7.21-7.31 (m, 11H), 7.04 (d, J = 7.2, 4H), 4.30 (t, J = 7.2, 2H), 1.83-1.90 (m, 2H), 1.38-1.44 (m, 2H), 0.96 (t, J = 7.2, 3H). **^{13}C NMR (100 MHz, $CDCl_3$):** δ 158.24, 140.74, 140.49, 139.14, 134.40, 131.60, 130.94, 130.15, 130.12, 129.94, 129.84, 129.34, 128.63, 128.55, 124.37, 124.00, 122.65, 120.04, 113.77, 111.26, 109.24, 92.34, 87.66, 43.22, 31.22, 20.65, 13.97. **HRMS (ESI, m/z):** calcd for $C_{62}H_{43}N_3Na$ $(M+Na)^+$, 852.3355; found, 852.3354.

Preparation of fluorescent organic nanoparticles

2-CTPAN and 2,2'-CTPAN has been dissolved separately in THF at a concentration of 1 mg/mL. Then 5 μL of 2-CTPAN and 8 μL of 2,2'-CTPAN of the above solution have been added to a poor solvent (water) to dilute the solution so that the final concentration of the solution becomes 10^{-5} M. The final solutions have been stirred vigorously and within 10 min of shaking the colloidal fluorescent organic nanoparticles (FONPs) of 2-CTPAN and 2,2'-CTPAN has been formed.

Acknowledgements

S. M. and C. P. are thankful to the University Grant Commission (UGC), India for providing the research fellowship.

Keywords: AIEE • self-assembly • solvent dependent nanoprobes • staircase-shaped supramolecular association • bio-imaging

[1] X. Zhang, X. Zhang, L. Tao, Z. Chi, J. Xu, Y. Wei, *J. Mater. Chem. B* **2014**, *2*, 4398–4414.
[2] K. Mandal, D. Jana, B. K. Ghorai, N. R. Jana, *J. Phys. Chem. C* **2016**, *120*, 5196–5206.
[3] X. Zhang, S. Wang, L. Xu, L. Feng, Y. Ji, L. Tao, S. Li, Y. Wei, *Nanoscale* **2012**, *4*, 5581–5584.
[4] X. Zhang, K. Wang, M. Liu, X. Zhang, L. Tao, Y. Chen, Y. Wei, *Nanoscale* **2015**, *7*, 11486–11508.
[5] O. S. Wolfbeis, *Chem. Soc. Rev.* **2015**, *44*, 4743–4768.
[6] I. L. Medintz, H. T. Uyeda, E. R. Goldman, H. Mattoussi, *Nat. Mater.* **2005**, *4*, 435–446.
[7] H. S. Choi, B. I. Ipe, P. Misra, J. H. Lee, M. G. Bawendi, J. V. Frangioni, *Nano Lett.* **2009**, *9*, 2354-2359.
[8] H. Sugimoto, M. Fujii, Y. Fukuda, K. Imakita, K. Akamatsu, *Nanoscale* **2014**, *6*, 122–126.
[9] F. Erogbogbo, K. T. Yong, I. Roy, G. X. Xu, P. N. Prasad, M. T. Swihart, *ACS Nano* **2008**, *2*, 873–878.
[10] P. Khandelwal, P. Poddar, *J. Mater. Chem. B* **2017**, *5*, 9055-9084.
[11] T. J. Mullen, M. Zhang, W. Feng, R. J. El-khouri, L. D. Sun, C. H. Yan, T. E. Patten, G. Liu, *ACS Nano* **2011**, *5*, 6539–6545.
[12] Q. Wan, K. Wang, H. Du, H. Huang, M. Liu, F. Deng, Y. Dai, X. Zhang, Y. Wei, *Polym. Chem.* **2015**, *6*, 5288-5294.
[13] S. M. Ng, M. Koneswaran, R. Narayanaswamy, *RSC Adv.* **2016**, *6*, 21624–21661.
[14] R. N. Day, M. W. Davidson, *Chem. Soc. Rev*. **2009**, *38*, 2887-2921.
[15] I. Roy, T. Y. Ohulchanskyy, H. E. Pudavar, E. J. Bergey, A. R. Oseroff, J. Morgan, T. J. Dougherty, P. N. Prasad, *J. Am. Chem. Soc.* **2003**, *125*, 7860-7865.
[16] K. Li, B. Liu, *Chem. Soc. Rev.* **2014**, *43*, 6570-6597.
[17] C. Xue, Y. Xue, L. Dai, A. Urbas, Q. Li, *Adv. Optical Mater.* **2013**, *1*, 581–587.
[18] K. M. Rajeshwar, E. Osugi, W. Chanmanee, C. R. Chenthamarakshan, M. V. B. Zanoni, P. Kajitvichyanukul, R. K. Ayer, *J. Photochem. Photobiol. C* **2008**, *9*, 171-192.
[19] E. K. L. Yeow, S. M. Melnikov, T. D. M. Bell, F. C. D. Schryver, J. Hofkens, *J. Phys. Chem. A* **2006**, *110*, 1726-1734.
[20] D. Xiao, L. Xi, W. Yang, H. Fu, Z. Shuai, Y. Fang, J. Yao, *J. Am. Chem. Soc.* **2003**, *125*, 6740-6745.
[21] W. Qin, D. Ding, J. Liu, W. Z. Yuan, Y. Hu, B. Liu, B. Z. Tang, *Adv. Funct. Mater.* **2012**, *22*, 771-779.

[22] J. Zhang, R. Chen, Z. Zhu, C. Adachi, X. Zhang, C. S. Lee, *ACS Appl. Mater. Interfaces* **2015**, *7*, 26266-26274.
[23] L. Wang, H. Dong, Y. Li, C. Xue, L. D. Sun, C. H. Yan, Q. Li, J. Am. Chem. Soc. 2014, 136, 4480−4483.
[24] Z. Zhao, J. W. Y. Lamb, B. Z. Tang, *J. Mater. Chem.* **2012**, *22*, 23726–23740.
[25] Z. Ning, Z. Chen, Q. Zhang, Y. Yan, S. Qian, Y. Cao, H. Tian, *Adv. Funct. Mater.* **2007**, *17*, 3799-3807.
[26] W. Qin, Z. Yang, Y. Jiang, J. W. Y. Lam, G. Liang, H. S. Kwok, B. Z. Tang, *Chem. Mater.* **2015**, *27*, 3892−3901.
[27] M. R. Molla, S. Ghosh, *Chem. Eur. J.* **2012**, *18*, 9860-9869.
[28] J. Li, K. Shi, M. Drechsler, B. Z. Tang, J. Huang, Y. Yan, *Chem. Commun.* **2016**, *52*, 12466-12469.
[29] Z. Zhao, B. He, B. Z. Tang, *Chem. Sci.* **2015**, *6*, 5347–5365.
[30] Y. Yuan, B. Liu, *ACS Appl. Mater. Interfaces* **2014**, *6*, 14903−14910.
[31] S. K. Lanke, N. Sekar, *Dyes Pigm.* **2016**, *124*, 82-92.
[32] S. Liu, H. Sun, Y. Ma, S. Ye, X. Liu, X. Zhou, X. Mou, L. Wang, Q. Zhao, W. Huang, *J. Mater. Chem.* **2012**, *22*, 22167–22173.
[33] Y. Chen, H. Liang, J. Photochem. Photobiol. **2014**, *135*, 23–32.
[34] C. Zhang, S. Jin, S. Li, X. Xue, J. Liu, Y. Huang, Y. Jiang, W. Q. Chen, G. Zou, X. J. Liang, *ACS Appl. Mater. Interfaces* **2014**, *6*, 5212−5220.
[35] X. Zhang, X. Zhang, S. Wang, M. Liu, L. Tao, Y. Wei, *Nanoscale* **2013**, *5*, 147-150.
[36] C. W. T. Leung, Y. Hong, S. Chen, E. Zhao, J. W. Y. Lam, B. Z. Tang, *J. Am. Chem. Soc.* **2013**, *135*, 62−65.
[37] Y. Yuan, S. Xu, X. Cheng, X. Cai, B. Liu, *Angew. Chem. Int. Ed.* **2016**, *55*, 6457-6461.
[38] M. Gao, Q. Hu, G. Feng, N. Tomczak, R. Liu, B. Xing, B. Z. Tang, B. Liu, *Adv. Healthcare Mater.* **2014**, *4*, 659-663.
[39] N. V. Lakshmi, T. M. Babu, E. Prasad, *Chem. Commun.* **2016**, *52*, 617-620.
[40] W. Dong, J. Pina, Y. Pan, E. Preis, J. S. S. Melo, U. Scherf, *Polymer* **2015**, *76*, 173-181.
[41] Y. Zhan, P. Gong, P. Yang, Z. Jin, Y. Bao, Y. Li, Y. Xu, *RSC Adv.* **2016**, *6*, 32697-32704.
[42] H. Kar, D. W. Gehrig, F. Laquai, S. Ghosh, *Nanoscale* **2015**, *7*, 6729-–6736.
[43] P. Lasitha, E. Prasad, *RSC Adv.* **2015**, *5*, 41420-41427.
[44] M. Gao, B. Z. Tang, *ACS Sens.* **2017**, *2*, 1382−1399.
[45] P. Sk, A. Chattopadhyay, *RSC Adv.* **2014**, *4*, 31994–31999.
[46] N. Lin, Q. Zhang, X. Xia, M. Liang, S. Zhang, L. Zheng, Q. Cao, Z. Ding, *RSC Adv.* **2017**, *7*, 21446–21451.
[47] R. T. K. Kwok, C. W. T. Leung, J. W. Y. Lam, B. Z. Tang, *Chem. Soc. Rev.* **2015**, *44*, 4228-4238.
[48] X. Zhang, X. Zhang, B. Yang, J. Hui, M. Liu, Z. Chi, S. Liu, J. Xu, Y. Wei, *J. Mater. Chem. C* **2014**, *2*, 816–820.
[49] X. Zhang, X. Zhanga, B. Yang, J. Hui, M. Liu, Y. Wei, *Colloids Surf., B* **2014**, *116*, 739–744.
[50] N. Balsukuri, I. Gupta, *Dyes Pigm.* **2017**, *144*, 223-233.
[51] Y. Chang, C. Michelin, L. Bucher, N. Desbois, C. P. Gros, S. Piant, F. Bolze, Y. Fang, X. Jiang, K. M. Kadish, *Chem. Eur. J.* **2015**, *21*, 12018-12025.

10.1002/chem.201900312

Entry for the Table of Contents

Layout 1:

FULL PAPER

The carbazole and 2,3,3-triphenylacrylonitrile (TPAN) nano-structures(2-CTPAN and 2,2'-CTPAN) have been designed and synthesized which exhibit aggregation induced emission enhancement (AIEE) behaviour in water with high fluorescence quantum yield. Both the compounds show tunable self-assembly in water as well as in dimethylformamide (DMF) by extended π-π stacking interaction. 2-CTPAN and 2,2'-CTPAN form organogels in DMF and exhibit acicular and rod shaped morphology, respectively. The single crystal structure of 2-CTPAN shows that the intermolecular C-H ⋯π interactions lock the molecular conformation into a staircase-shaped supramolecular assembly. These AIEE active compounds are very efficient as bio-imaging agent.

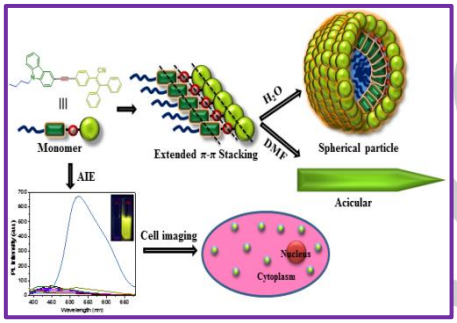

Santu Maity,[a] Krishnendu Aich,[a] Chandraday Prodhan,[b] Keya Chaudhuri,[b] Ajoy Kumar Pramanik,[c] Siddhartha Das,[d] and Jhuma Ganguly[a]*

Page No. – Page No.

Title